Astronomy & Astrophysics manuscript no. aa23083-13
December 11, 2014
©ESO 2014

arXiv:1412.0462v2 [astro-ph.GA] 10 Dec 2014

OH and H_2O maser variations in W33B

P. Colom[1], E. E. Lekht[2], M. I. Pashchenko[2], and G. M. Rudnitskij[2]

[1] LESIA, Observatoire de Paris, Section de Meudon, CNRS, UPMC, Université Paris-Diderot, 5 place Jules Janssen, 92195 Meudon CEDEX, France
e-mail: Pierre.Colom@obspm.fr
[2] Lomonosov Moscow State University, Sternberg Astronomical Institute, 13 Universitetskij prospekt, Moscow, 119234, Russia
e-mail: gmr@sai.msu.ru

Received: 19 November 2013 / accepted 22 October 2014

ABSTRACT

Context. The active star-forming region W33B is a source of OH and H_2O maser emission located in distinct zones around the central object.
Aims. The aim was to obtain the complete Stokes pattern of polarised OH maser emission and to trace its variability and to investigate flares and long-term variability of the H_2O maser and evolution of individual emission features.
Methods. Observations in the OH lines at a wavelength of 18 cm were carried out on the Nançay radio telescope (France) at a number of epochs in 2008–2014; H_2O line observations (long-term monitoring) at $\lambda = 1.35$ cm were performed on the 22-metre radio telescope of the Pushchino Radio Astronomy Observatory (Russia) between 1981 and 2014.
Results. We have observed strong variability of the emission features in the main 1665- and 1667-MHz OH lines as well as in the 1612-MHz satellite line. Zeeman splitting has been detected in the 1665-MHz OH line at 62 km s^{-1} and in the 1667-MHz line at 62 and 64 km s^{-1}. The magnetic field intensity was estimated to be from 2 to 3 mG. The H_2O emission features form filaments, chains with radial-velocity gradients, or more complicated structures including large-scale ones.
Conclusions. Long-term observations of the hydroxyl maser in the W33B region have revealed narrowband polarised emission in the 1612-MHz line with a double-peak profile characteristic of Type IIb circumstellar masers. The 30-year monitoring of the water-vapour maser in W33B showed several strong flares of the H_2O line. The observed radial-velocity drift of the H_2O emission features suggests propagation of an excitation wave in the masering medium with a gradient of radial velocities. In OH and H_2O masers some turbulent motions of material are inferred.

Key words. masers – ISM:molecules – ISM:radio lines – stars:formation

1. Introduction

Early studies showed that the thermal radio source W33 consists of two HII regions: strong and compact G12.80−0.20 and a fainter extended one G12.68−0.18 (see e.g. Goss & Shaver 1970). Subsequent observations by Goss et al. (1978) showed that the extended component (G12.80−0.18) in W33 consists of several faint discrete features. For the stronger source Gardner et al. (1975) found from H109α, H134α, and H158α radio recombination lines (RRL) radial velocities 35.8, 32.0 and 38.6 km s^{-1}, respectively. With this velocity the preferable kinematic distance to the W33 complex was believed to be 4.4 kpc (Haschick & Ho 1983). Quireza et al. (2006) observed toward W33 RRL C91α and C92α. The radial velocity of the extended region from the H134α line is 58 km s^{-1} (Gardner et al. 1975). The accepted model of the W33 region was an interstellar cloud expanding at a velocity of ∼13 km s^{-1}, thus producing in its radio line spectra two Doppler components at approximately 32 and 58 km s^{-1}.

Pandian et al. (2008) resolved the kinematic distance ambiguity for a number of galactic HII regions, among them W33, using 21 cm HI absorption spectra. For this purpose they employed a method proposed by Kolpak et al. (2003). From the absence of an HI absorption feature at the tangential-point velocity in the direction of W33 Pandian et al. (2008) concluded that W33 is at the near kinematic distance. They estimated its distance as 4.9–5.1 kpc with a probable error of ±0.6 kpc. Finally, Forster & Caswell (1989) give for W33B a somewhat larger distance of 6.4 kpc.

However, the latest measurement of the trigonometric parallax of H_2O masers in W33B (Immer et al. 2013) yields for this source a distance of $2.40^{+0.17}_{-0.15}$ kpc, thus placing it in the Scutum spiral arm. It was shown that all the maser sources in the W33 region, together with some nearby masers outlining the Scutum Arm (Sato et al. 2014), are interconnected and are at the same distance; the sources A and B possess proper motions with respect to C and to their central stars. The proper motions of the H_2O masers are discussed below.

Toward W33 three OH and H_2O maser emission sources are observed: W33 A, B, and C. The W33 A and B masers are arranged symmetrically relative to W33C and are at an angular distance of 7′.5 from it. Sources B and C are associated with the HII regions G12.68−0.18 and G12.80−0.20, respectively. Source A is at the periphery of the W33 region, near the faint feature G12.91−0.28 (Goss et al. 1978).

Send offprint requests to: P. Colom
A complete version of Figure 7 is available in electronic form from http://www.aanda.org/. OH and H_2O data in ASCII format are available at the CDS via anonymous ftp at cdsarc.u-strasbg.fr (130.79.128.5), http://cdsweb.u-strasbg.fr/cgi-bin/qcat?J/A+A/, or http://comet.sai.msu.ru/~gmr/Maser_monitoring/W33B/

Maser emission in the main OH lines 1665 and 1667 MHz was detected toward W33B by Goss (1968). It was observed in a velocity interval of 58–66 km s^{-1}. Robinson et al. (1970) made measurements in the main lines as well as in the 1612- and 1720-MHz satellite OH lines; they managed to detect only the main-line emission. The velocity coincidence of this HII region and the OH maser source testifies to their physical association.

In 1978 Pashchenko (1980) detected on the Nançay radio telescope thermal emission and absorption in the satellite OH lines toward W33B coming from a $\sim 7' \times 7'$ extended source (molecular cloud) as well as weakly polarised emission from a pointlike source in the 1612-MHz line. Observations in 1978 on the same radio telescope showed that the main-line OH emission is strongly polarised circularly. The emission (and absorption) in a velocity interval of 30–40 km s^{-1} belongs to the sources W33C and A, and in an interval of 55–65 km s^{-1} to the source W33B.

The H_2O maser emission was detected toward W33 by Genzel & Downes (1977) at virtually the same radial velocities as the OH emission. An exception is the emission at small negative velocities in W33C. In contrast to OH, a stronger H_2O source in this region is W33B. Subsequent observations (Jaffe et al. 1981, and this work) confirmed this characteristic of the H_2O masers.

The W33B region also hosts a strong source of maser emission of methanol (CH_3OH) in the $5_1 - 6_0 A^+$ 6.67-GHz rotational line (Menten 1991). The line profile consists of two peaks at $v_{LSR} \sim 52$ and 58 km s^{-1}.

According to the VLA observations of Forster & Caswell (1989, 1999) for most maser sources associated with star-forming regions, OH and H_2O masers occur in small groups with a diameter of less than 0.03 pc. They have a common source of energy, but are physically located in distinct zones.

2. Observations and data presentation

We observed the W33B radio source in the 18 cm hydroxyl lines at various epochs on the telescope of the Nançay Radio Astronomy Station of the Paris–Meudon Observatory (France). The method of observation and processing of data was presented by Slysh et al. (2010) and Lekht et al. (2012). At declination $\delta = 0°$ the telescope beam at a wavelength of 18 cm is $3'.5 \times 19'$ in right ascension and declination. The telescope sensitivity at $\lambda = 18$ cm and $\delta = 0°$ is 1.4 K/Jy. The system noise temperature of the helium-cooled front-end amplifiers is from 35 to 60 K depending on the observational conditions.

We observed H_2O maser emission in the 1.35 cm line toward W33B ($\alpha_{2000} = 18^h13^m54^s.7$, $\delta_{2000} = -18°1'46''.5$) on the 22-metre radio telescope in Pushchino from February 1981 to January 2014 with a half-power beamwidth of $2'.6$. In the observations of this source the system noise temperature with a helium-cooled field-effect transistor (FET) front-end amplifier was 120 – 270 K depending on the weather conditions. The signal spectrum was measured by a 128-channel filter-bank analyser with a velocity resolution of 0.101 km s^{-1}, and since the end of 2005 by a 2048-channel autocorrelator with a resolution of 0.0822 km s^{-1}. For a pointlike source an antenna temperature of 1 K corresponds to a flux density of 25 Jy.

Figure 1 presents the results of observations of hydroxyl maser emission in the 1665- and 1667-MHz lines. The observations in 2008 were carried out with a velocity resolution of 0.137 km s^{-1}, and those of 2010–2014 with a resolution of 0.068 km s^{-1}. The technique of the observations was described in detail by Pashchenko et al. (2009) and Slysh et al. (2010).

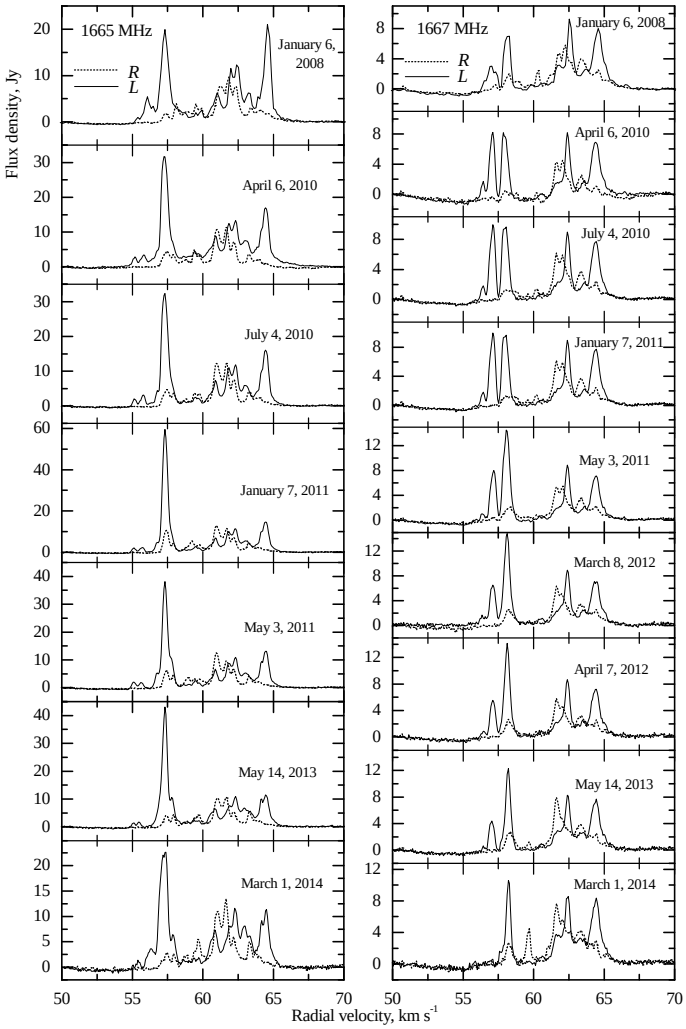

Fig. 1. Spectra of OH maser emission in the 1665- and 1667-MHz lines at various epochs. Solid curves: left-hand circular polarisation; dashed: right-hand circular.

Figures 2 and 3 show Stokes parameters for the main lines at 1665 and 1667 MHz at the epochs of January 6, 2008, and May 3, 2011. Figure 4 presents central parts of the spectra for Stokes parameter V of the OH main lines at different epochs. The main spectral features are numbered. The results of our observations in the 1612- and 1720-MHz satellite lines are presented in Figures 5 and 6, respectively.

Figure 7 represents an atlas of the H_2O spectra for the interval from November 1981 to January 2014. For technical reasons, no observations were conducted between May 2006 and December 2007. The horizontal axis is the velocity relative to the local standard of rest (LSR). All the spectra are given in the same radial-velocity scale. An arrow at the vertical axis shows the scale in janskys. In the spectra zero baselines have been drawn.

Superpositions of the H_2O spectra for various time intervals (1–6) are shown in Figure 8. The separation was done according to the character of the spectral evolution. Averaged spectra are shown with bold curves. The maser emission in the velocity interval of 55 – 63 km s^{-1} is observed during two time intervals (1 and 3). At the rest time the emission is observed mainly in one or two narrow velocity intervals, 55 – 57.5 and 58 – 62 km s^{-1}. From 2001 to 2012 the velocity centroid of the averaged spectra of the main group (58 – 62 km s^{-1}) moved from

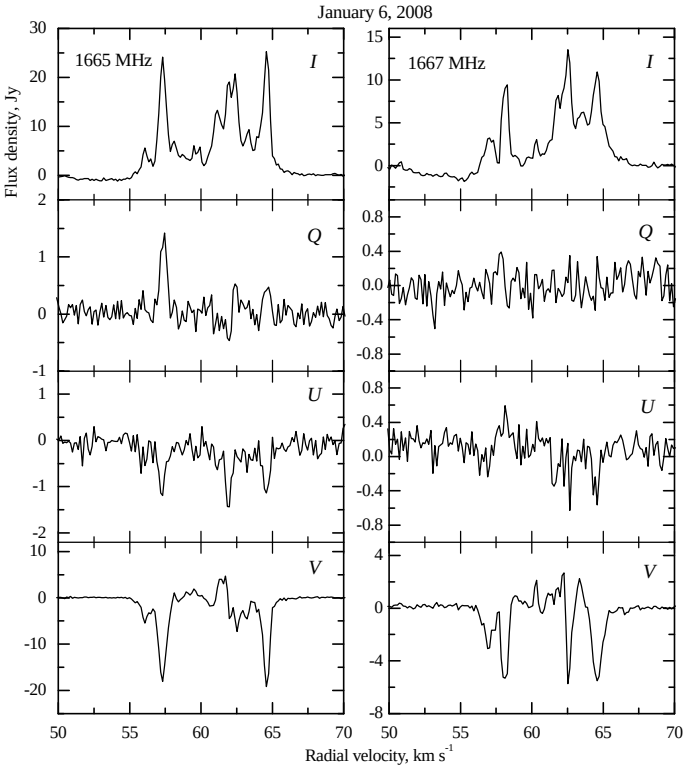

Fig. 2. Stokes parameters of the main lines at 1665 and 1667 MHz for the epoch January 6, 2008.

60.4 to 59.4 km s^{-1}. In addition, fluctuations of the velocity centroid calculated for individual spectra were observed.

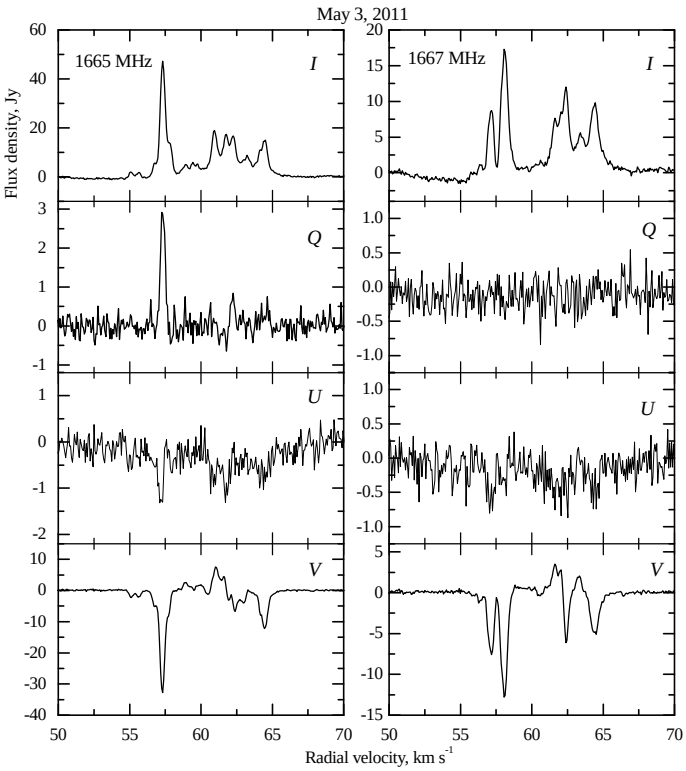

Fig. 3. Same as in Fig. 2, for the epoch May 3, 2011.

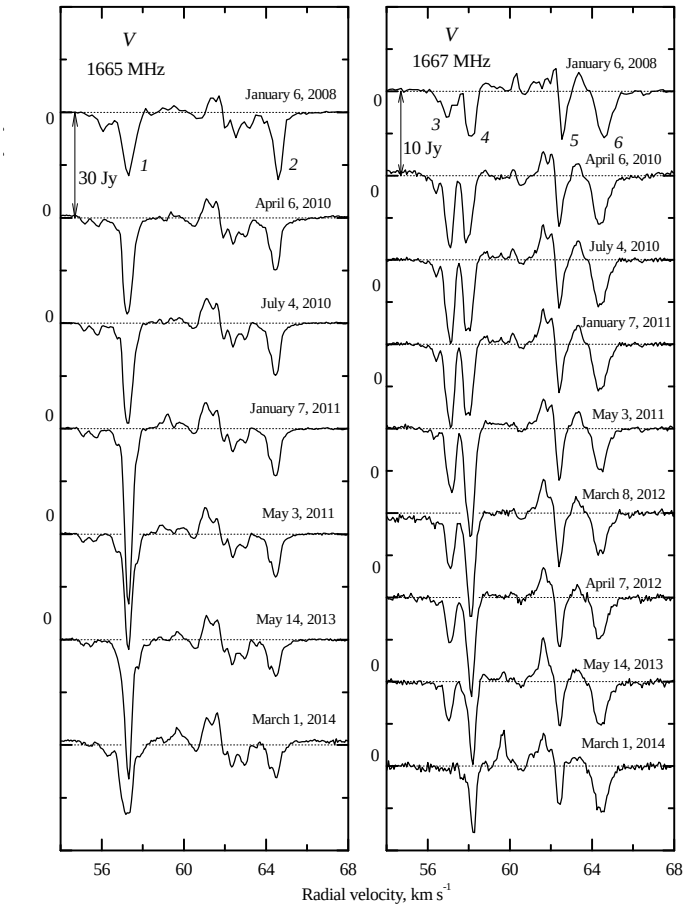

Fig. 4. Central parts of the OH main-line spectra for the Stokes parameter *V* for various epochs of the observations. Main spectral features are numbered.

3. Data analysis and discussion

3.1. Hydroxyl

In 1978, using high angular resolution in right ascension of the Nançay radio telescope, we searched for the emission/absorption peaks in the satellite OH lines. Figure 9 shows the emission/absorption intensity as a function of right ascension for different spectral features. Vertical arrows denote positions of radio continuum peaks (W33C and B). Features 1 (62.3 km s^{-1}) and 2 (56 km s^{-1}) are unresolved, whereas feature 3 (~50 km s^{-1}) is extended. Peaks of features 1 and 2 in the 1612-MHz line do not coincide; the former is detectable only in the 1612-MHz line and can be associated with a maser spot.

Thus, according to our observations in 1978, 1991, 2012, and 2014, (thermal) emission/absorption satellite-line features in the velocity interval 49–58 km s^{-1} belong to an extended source, whereas narrow emission features come from a pointlike source.

Of interest is broadband absorption in the main OH lines, which probably covers the entire velocity interval filled by OH maser emission features. It is visible at the *I* profile edges and, probably, in the *U* Stokes profile (Figures 2 and 3), thus suggesting a slight linear polarisation. The velocity range can be assessed more certainly in the OH satellite lines, especially in 1720 MHz, where OH is partly in thermal emission and partly in absorption (see Figures 5 and 6). It covers radial velocities $V_{LSR} \approx$ 50–65 km s^{-1}, which probably represent the entire velocity dispersion of material in the molecular cloud surrounding the W33B maser.

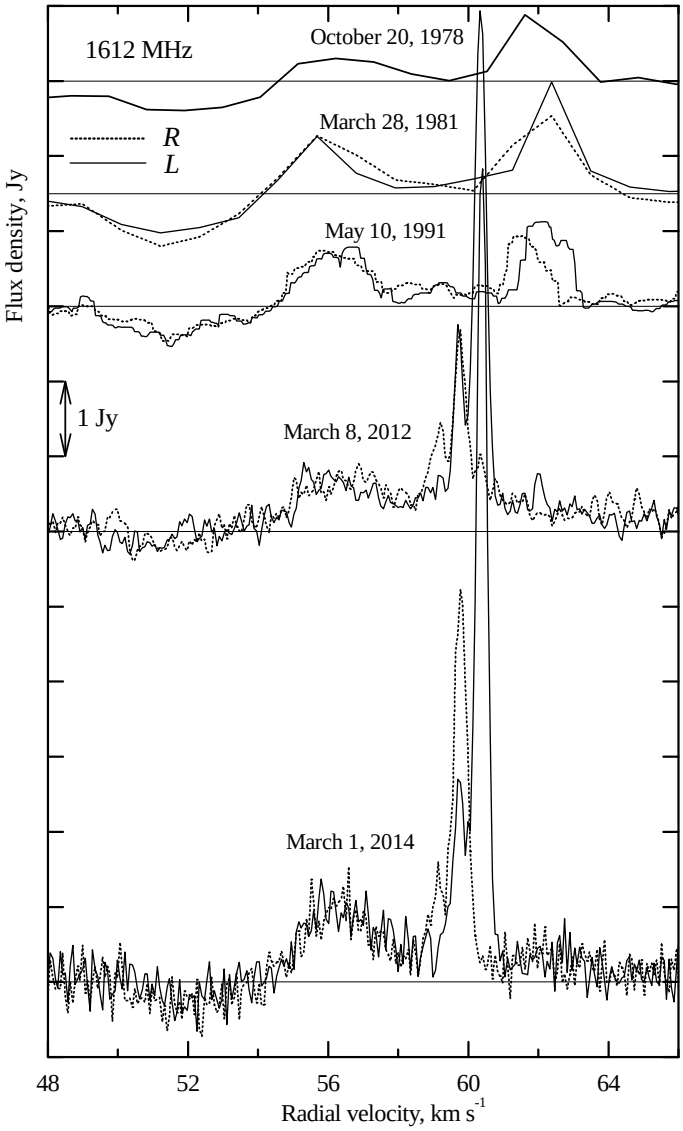

Fig. 5. Spectra of OH maser emission in the satellite line at 1612 MHz. Spectra in right- and left-hand circular polarisation are shown with dotted and solid lines, respectively. Strong narrowband polarised maser emission is visible in the 2012 and 2014 profiles.

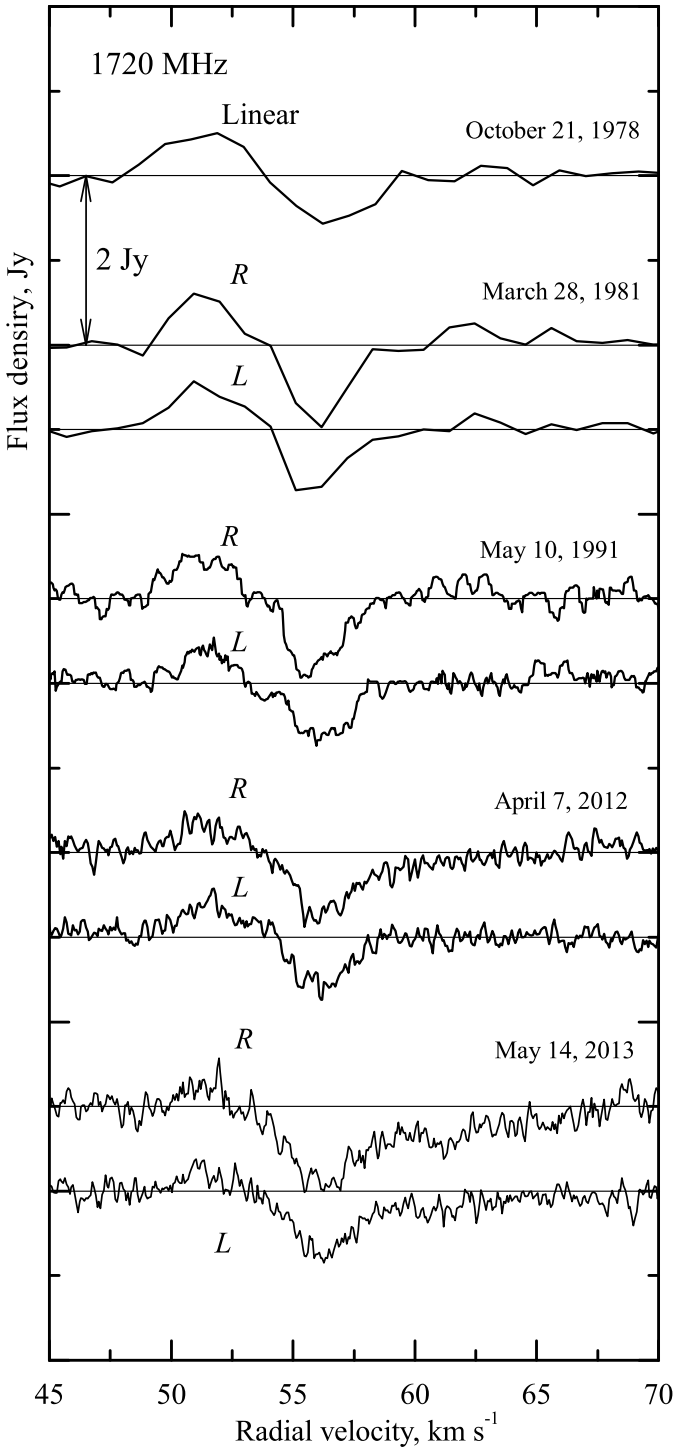

Fig. 6. Spectra of OH maser emission in the satellite line at 1720 MHz. There is no difference between right- (*R*) and left-hand (*L*) polarised profiles.

3.1.1. The structure of the OH maser source

Figure 10a shows the arrangement of the main-line OH masers spots for the epoch 1991 (Argon et al. 2000). Spots' radial velocities are indicated. The angular size of the main-line masering region is 0.4×0.4 arcsec; the regions of emission in the 1665- and 1667-MHz lines are spatially separated. The map centre ΔRA = 0, ΔDec = 0 corresponds to RA(2000)=$18^{h}13^{m}54.75^{s}$, Dec(2000)=$-18°1'46.4''$. The distribution of the maser spots is delineated with arcs (dashed curves). We observe regular radial-velocity variations along the arc for the 1665-MHz maser spots. At first, the velocity decreases, then increases. There are several clusters of maser spots with a small V_{LSR} dispersion. An asterisk marks the presumed location of the central star for the OH maser source based on the arc shape i.e. on the large-scale structure of the source. Another argument supporting our supposition is the large separation between the OH and H_2O masers in W33B. In contrast to Forster & Caswell (1989), we think that each maser has its own source of energy.

3.1.2. Main-line emission

The OH maser in W33 B is a typical representative of hydroxyl masers associated with star-forming regions: the 1665-MHz line is stronger than the 1667-MHz line.

Our main-line observations have shown that most OH emission features in W33 B have a high degree of circular polarisation (see Figure 1). Another peculiarity of the OH spectra is

strong variability of the most intense features. We have found no Zeeman splitting for such features.

For the detection and study of Zeeman components we use Stokes parameter V, the difference of the right- and left-hand circular polarisations (see Figures 2–4). In the 1665-MHz line the σ Zeeman components can be a pair of spectral features near 62 km s^{-1}, and in the 1667-MHz line these are pairs of features near 62 and 64 km s^{-1}. The splitting is 1.3, 0.7 and 1.1 km s^{-1}. This corresponds to intensities of the line-of-sight magnetic field of $B = -2.2, -2.0$ and -3.1 mG, respectively ($B < 0$ corresponds to the field directed toward the observer).

It should be emphasised that in both OH main lines at 62 km s^{-1} we have obtained quite similar field intensities, -2.2 and -2.0 mG. These features may be produced by the same maser condensation.

As for previous measurements of the magnetic field toward W33 B, Zheng (1991), who observed W33B on the 43-m NRAO radio telescope in October 1981, found an average field $B = -5$ mG from the shifts of the mean weighted velocities in the both main OH lines 1665 and 1667 MHz. Fish et al. (2003) found in their VLA observations of August 1991 several Zeeman pairs of right- and left-hand circularly polarised features within a velocity interval of 62.5–64.5 km s^{-1} in both OH main lines. Their estimates for the field strength are from -0.7 to -7.5 mG. The quoted estimates do not contradict ours, both in the field direction and in the order of magnitude. The direction of the magnetic field fits the general field pattern in the Scutum Arm as directed counterclockwise when viewed from the north galactic pole. Thus, during the collapse of the protostellar gas cloud the general direction of the interstellar field could have been conserved.

3.1.3. Satellite-line emission

As in the source W33C in the same region (Colom et al. 2012), the profiles of the 1612- and 1720-MHz OH lines toward W33B (Figures 5, 6) consist of emission and absorption components and mirror each other: peak velocities are, respectively, 56.15 and 51.66 km s^{-1} in the 1612-MHz line, 51.47 and 56.23 km/s in the 1720-MHz line. The mean difference is 4.6 km s^{-1} (for W33C it is 3.4 km s^{-1}).

This structure is explained in a model of an OH source associated with a molecular cloud where a maser is embedded in. If an IR source is present in the cloud its radiation affects the populations of the hyperfine structure sublevels of OH molecules (Burdyuzha & Varshalovich 1973). In this model particulars of the IR pumping are such that inversion of the 1720-MHz transition levels is accompanied by anti-inversion in the 1612-MHz transition and vice versa. The inversion or anti-inversion is determined by the angle between the direction of propagation of the IR radiation and the direction of local magnetic field. For a source embedded in the cloud one of the satellites is inverted and the other one is anti-inverted; in the other part of the cloud the situation is the opposite. This effect was observed by us in W33C (Figure 9).

In 2012 we detected narrowband 1612-MHz maser emission in both circular polarisations. In 1991 this emission was absent. We detected three emission features at radial velocities 59.1, 59.7 and 60.4 km s^{-1}. Table 1 lists their flux densities at different epochs. The columns labelled F_R and F_L contain flux densities in the right- and left-hand circular polarisations, respectively; the columns labelled p list degree of polarisation $p = |F_R - F_L| / (F_R + F_L)$.

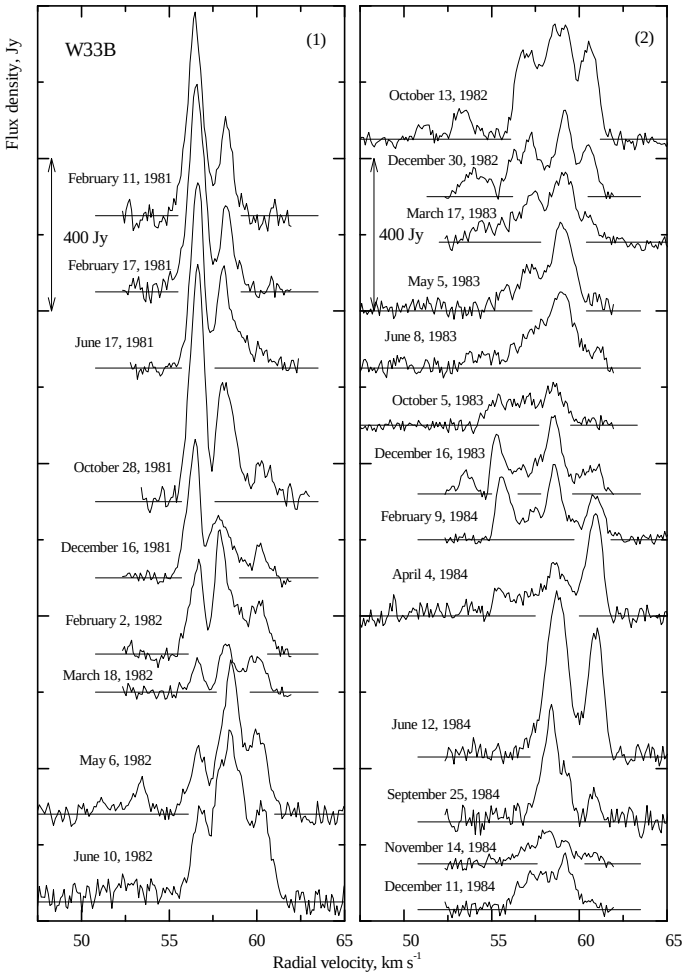

Fig. 7. Spectra of the H_2O maser emission in W33B.

Table 1. Flux densities in the right- (F_R) and left-hand (F_L) circular polarisations in janskys and the degree of polarisation p in the 1612-MHz OH line.Typical 1σ errors are about 0.1 Jy.

Date	Radial velocity, km s^{-1}								
	59.1			59.8			60.4		
	F_R	F_L	p	F_R	F_L	p	F_R	F_L	p
2012 Mar 8	1.4	0.3	0.65	2.7	2.6	0.02	1.0	6.9	0.75
2012 Apr 7	1.6	0	1	3.7	2.5	0.19	0.3	7.5	0.92
2012 Sept 7	1.7	0	1	4.5	2.8	0.23	0.6	9.4	0.88
2013 May 14	1.5	0	1	5.5	3.4	0.24	0.7	10.6	0.88
2014 Mar 1	1.5	0	1	5.1	2.6	0.32	0.3	10.7	0.95

The emission at 59.8 and 60.4 km s^{-1} is variable, and the degree of polarisation also varies. The cause of this can be turbulent motions of material in the masering region. The observed emission components have no strong counterparts either in the main OH lines or in the 1720-MHz satellite line. Thus, we may observe a new Type IIb OH maser probably associated with an infrared star. However, the radial-velocity range (~1.3 km s^{-1}) is too narrow as compared to typical values for OH masers in late-type giants and supergiants, from 5 km s^{-1} up to 40 km s^{-1}. The 1612-MHz emission features being within the velocity interval of the main-line emission suggests the same distance and physical association with the 1665/1667-MHz maser. Very long baseline interferometry (VLBI) observations would be desirable to resolve this question.

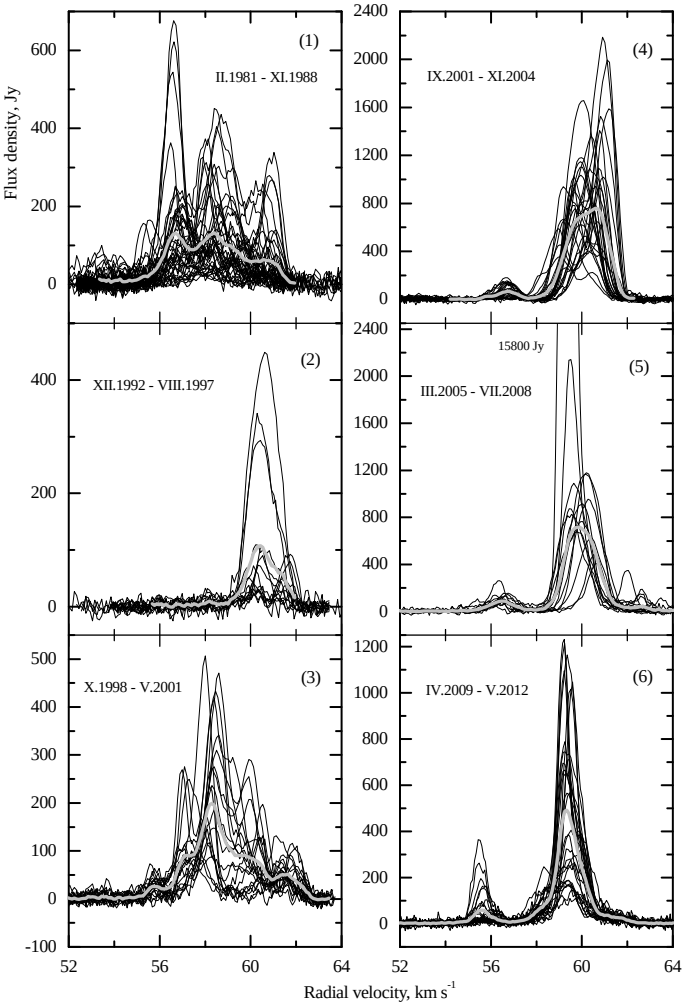

Fig. 8. Superposition of the H_2O 22-GHz spectra for various time intervals. The separation was done according to the character of the spectral evolution. Averaged spectra for the intervals are shown with bold light curves. See text for details.

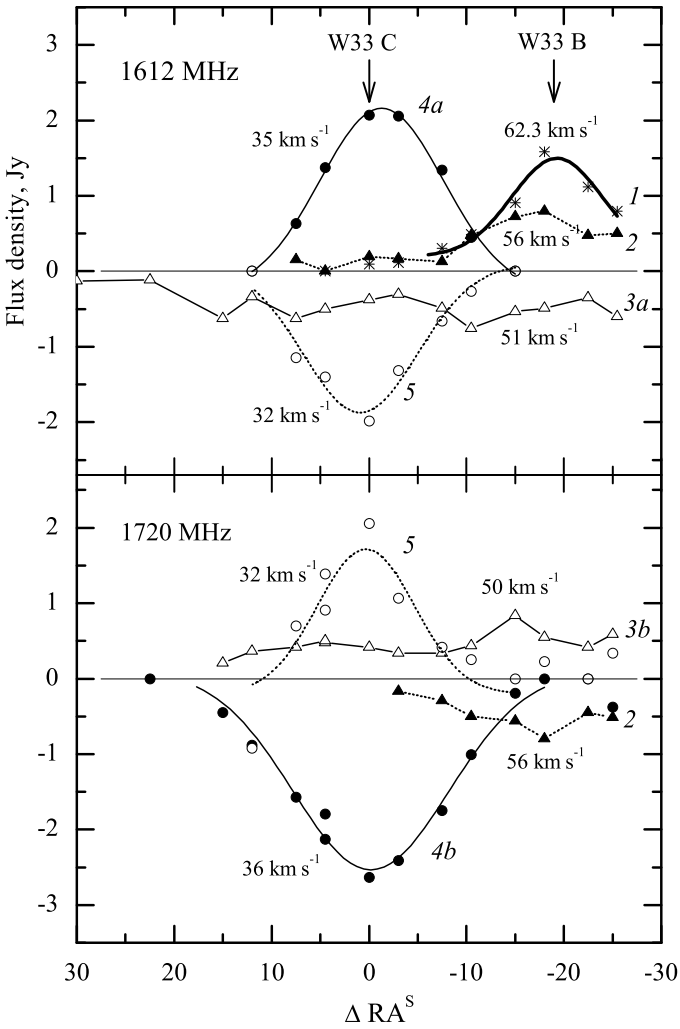

Fig. 9. Flux density of the features in the satellite OH lines as a function of right ascension toward W33. Δ RA=0 corresponds to the position of W33C. Features with similar radial velocities are designated *3a*, *4a* and *3b*, *4b* in the 1612- and 1720-MHz lines, respectively. The strong 1612-MHz maser feature at 62.3 km s^{-1} (shown with bold line in the upper panel) certainly belongs to W33B.

3.2. Water-vapour emission

On the basis of our regular long-term monitoring of W33B performed with a high spectral resolution, we have studied both fast and long-term variations of H_2O maser emission as well as the evolution of individual features.

Figure 11 shows variations of the integrated H_2O line flux. The point marked (×) is from Lada et al. (1981) and (△) is from Jaffe et al. 1981. Two stages of maser activity are prominent. Arrows mark the epochs of the interferometric observations.

We find no cyclicity in the maser variability. We observed two deep minima: in 1989–1990 and in mid-1997. In addition, we observed flare-type variability.

There were several interferometric observations of the H_2O maser in W33B. In January 1979 W33B was observed for the first time by VLBI in the 22-GHz H_2O line by Lada et al. (1981) with a baseline of 845 km. Their map contains four maser features within a region ∼ 0.05″ i.e. 120–250 AU depending on the accepted distance, 2.4 or ∼5 kpc (see Introduction).

In June 1984, Forster & Caswell (1989) observed W33B on VLA with a spatial resolution of about 3″ and radial velocity resolution of 1.32 km s^{-1}. The estimated size of the region hosting maser spots (except for one) is 0.06″ × 0.07″ (300×350 AU) in the right ascension and declination, respectively (see Figure 10b). The map centre ΔRA = 0, ΔDec = 0 corresponds to RA(2000)=$18^h13^m54.7^s$, Dec(2000)=−18°1′48.0″. The maser spots are plotted with filled circles. The radial velocities of each maser spot are indicated. The presence of a radial-velocity gradient is visible, its direction is shown with a dashed line. A horizontal bar shows the linear scale of the W33B region.

Immer et al. (2013) observed H_2O masers in the W33 complex on VLBA at nine epochs between September 2010 and January 2012. In addition to the trigonometric parallax yielding a distance of 2.4 kpc, they found proper motions of individual H_2O maser features in W33B that are within 4 mas/year. We note that such proper motions correspond to projected velocities in the sky plane of ∼45 km s^{-1}, which are by a factor of a few larger than the maximum line-of-sight velocity spread (∼10 km s^{-1}, see Figure 8). This is at variance with the model of spherically symmetric expansion; the cause of this difference is not yet clear.

We have identified main spectral components of our monitoring (for the period June 1984) with the VLA map components. This is shown with arrows in the left panel of Figure 12. Since the spectral resolution of our monitoring is considerably higher, we have identified and traced the evolution of a larger number of

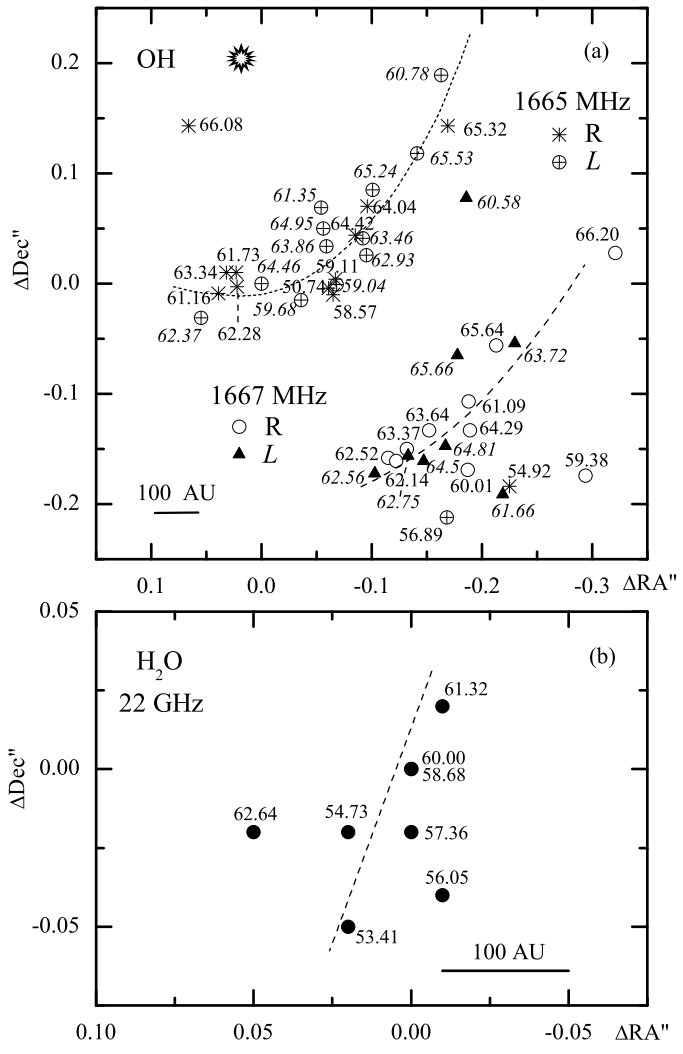

Fig. 10. (a) VLA map of main-line OH masers for the epoch 1991 (Argon et al. 2000). Right- and left-hand polarised features are shown with different symbols. Spots' radial velocities are indicated, those of left-hand polarised features are in *italics*. An asterisk marks the presumed location of the central star for the OH maser source based on the arc shape.
(b) Positions of VLA H_2O maser spots in June 1984 (Forster & Caswell 1999) On both maps the 100 AU bar corresponds to the trigonometric distance of 2.4 kpc (Immer et al. 2013). Spots' radial velocities are indicated. Dotted curves show the preferential direction of the growth of the spots' radial velocities.

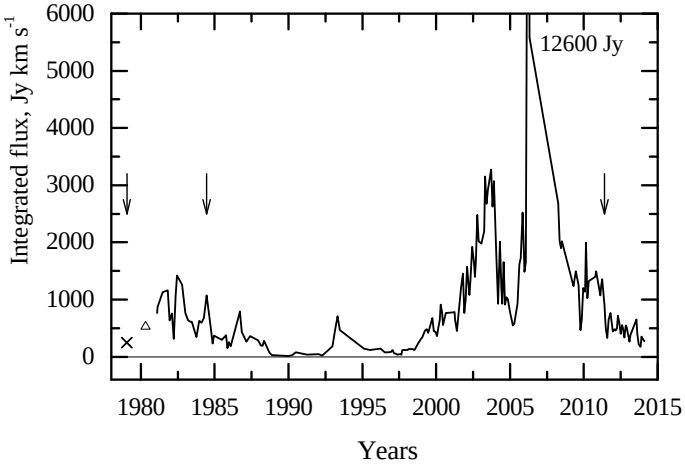

Fig. 11. Variations of the integrated H_2O line flux. Two points at the left taken from observations of other authors: (×) from Lada et al. (1981) and (△) from Jaffe et al. 1981. Arrows mark the epochs of the interferometric observations.

H_2O emission features than the VLA maps. Thus, each feature on the VLA map may actually correspond to a cluster of several maser spots. The V_{LSR} gradient testifies that the clusters of maser spots form a large-scale organised structure.

Since 2000 the H_2O maser was quite active in the radial-velocity interval 58–62 km s^{-1}, with an intermediate minimum in early 2005. Since mid-2011 the activity has declined. In the quoted activity interval we observed flares of individual features as well as of groups of features. The strongest flare took place in 2006. In March the flux density reached almost 16,000 Jy.

Figure 12 (right-hand panel) shows radial-velocity variations of the strongest emission features in W33B. For each of them circles of different sizes mark the emission maxima in which the flux density exceeded 700 Jy. The circle size corresponds to the flux density magnitude. For all maxima flux densities are given in janskys. In 2000–2003 the emission maximum was moving toward higher velocities and then in the opposite direction (dashed curves). This may be due to an ordered arrangement of maser condensations such as clusters, fragments of shells, etc. This result is consistent with the H_2O structure on the VLA map (Forster & Caswell 1999) as well as with the map of Immer et al. (2013).

The strongest flare at 59.4 km s^{-1} in the beginning of 2006 was preceded by complicated variations in the spectrum structure and by a shift of the emission peak from 60.6 to 59.4 km s^{-1}. At the epoch of the maximum the line profile was gaussian. The line was symmetric, its width at half-maximum was 0.53 km s^{-1}. It was local, and it might be associated with a maser spot. In the presence of turbulent or chaotic motions of maser condensations in a cluster, two clumps of material can become superposed in the line of sight, which results in an increase in the optical depth τ of the medium. For instance, in the case of the unsaturated maser an increase in τ by a factor of 2.3 results in an intensity growth by an order of magnitude.

In some time intervals we observed appreciable radial-velocity variations of the H_2O emission features. Most likely, each feature is identified not with an individual maser spot but with some structure, for instance, a filament, a chain with a radial-velocity gradient or with a more complex formation; see e.g. Torrelles et al. (2003), Lekht et al. (2007). We observed the emission from such structures during intervals of high activity of the maser source, often in the periods of flare activity. During propagation in the masering medium of a shock wave driven by the stellar wind or molecular outflow, regions with different radial velocities are consecutively excited. This results in the spectral and spatial drift of the observed emission peak. In addition, we observed an appreciable radial-velocity drift of the emission for the cluster of maser spots from 57.5 to 55.5 km s^{-1} (dashed line in Figure 12b). The drift is indeed considerable to take into account that the radial-velocity dispersion of all maser spots in W33B does not exceed 8 km s^{-1}. The drift time interval falls on the stage of maximum H_2O maser activity in W33B. This is confirmed by the proper motions of the maser condensations found by Immer et al. (2013).

The complicated character of the radial-velocity variations may reflect the presence of turbulent motions of material within an H_2O maser condensation as well as on the scale of compact clusters of maser spots.

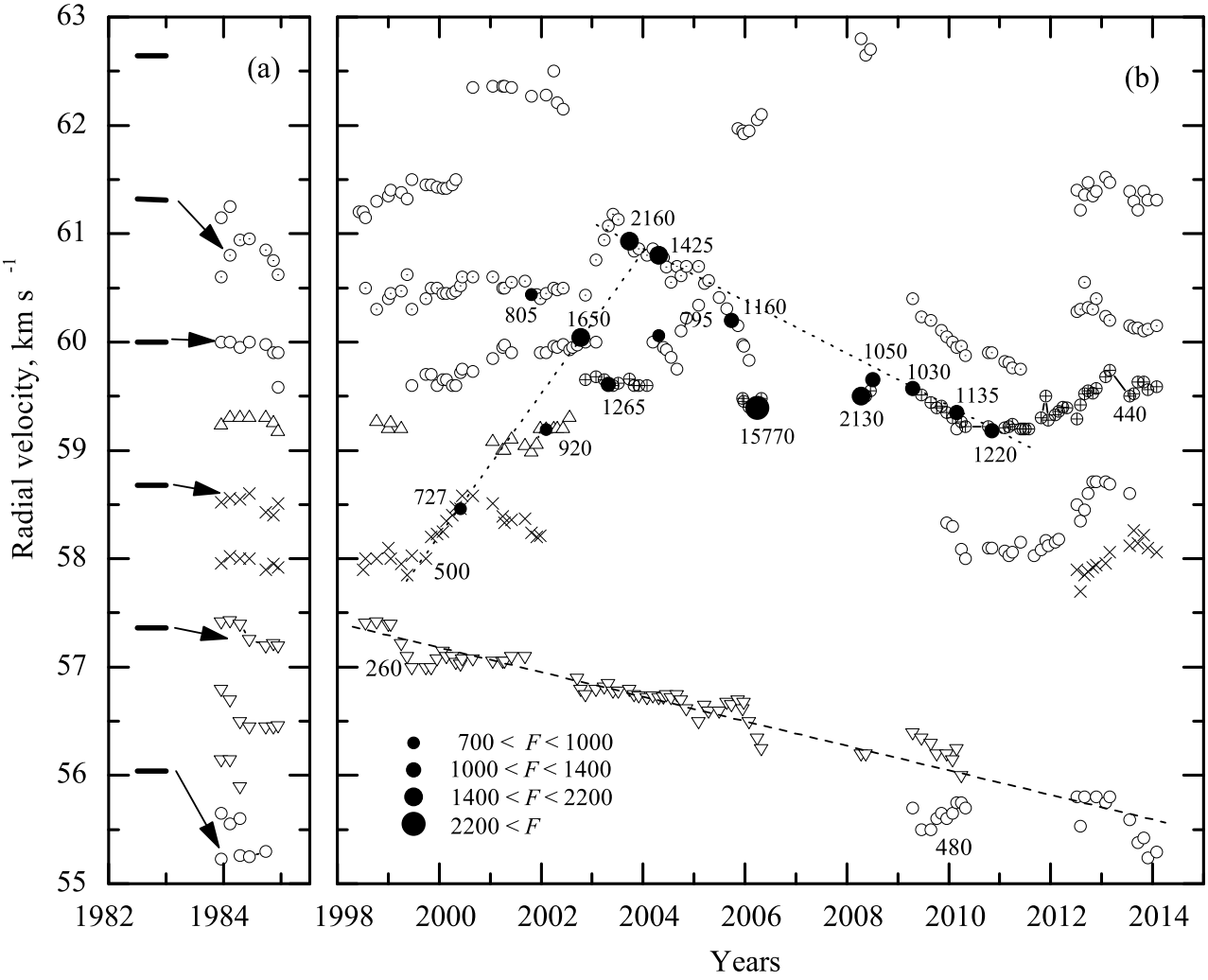

Fig. 12. Radial-velocity variations of the strongest H_2O emission features in W33B. Peaks at different velocities are shown with different symbols. Main features are shown with circles of different kinds. Circles of various sizes denote emission peaks with flux densities that exceeded 700 Jy. The circle size corresponds to the flux density magnitude. For each peak its flux density is given in janskys. Dashed and dotted lines (drawn by eye) present probable radial-velocity drifts of features persisting throughout our monitoring. Characteristic timescales are of the order of months.

4. Summary

We list the main results of our long-term observations of the hydroxyl maser and of the 30-year monitoring of the water-vapour maser in the source W33 B.

1. We have observed strong variability of the emission features in the main OH lines 1665 and 1667 MHz.
2. We have detected Zeeman splitting σ-components in the 1665-MHz OH line at 62 km s^{-1} and in the 1667-MHz line at 62 and 64 km s^{-1}. From the amount of splitting we have estimated the line-of-sight component of the magnetic field for each of the masering regions as 2.0–2.2 and 3.1 mG, respectively.
3. The profiles of the satellite lines at 1612 and 1720 MHz mirror each other. This suggests pumping of the levels of these transitions by infrared emission of the source embedded in the magnetised interstellar cloud around the maser.
4. We have detected narrowband, strongly variable emission in the 1612-MHz line with a high degree of circular polarisation, which belongs to a pointlike source.
5. We present an atlas of the H_2O λ = 1.35 cm emission spectra toward W33 B for the time interval from November 1981 to May 2006 and from December 2007 to January 2014. The mean interval between consecutive observational sessions was 2.2 months. The radial-velocity resolution was 0.101 km s^{-1}, and since the end of 2005 it was 0.0822 km s^{-1}.
6. We detected flares of individual H_2O spectral features and of groups of features (clusters). The emission features probably form filaments, chains with a radial-velocity gradient, or more complicated structures including large-scale ones.
7. The characteristic variations of OH and H_2O maser emission suggest the existence of turbulent motions of material in the regions of the maser spots' localisation.
8. We have observed two stages of activity of the H_2O maser with an interval between the main maxima of about 20 years.
9. The arc-like arrangement of the OH maser spots and the large separation between the OH and H_2O maser sources allow us to suppose that the hydroxyl and water vapour masers have independent energy sources.

Acknowledgements. The Nançay Radio Observatory is the Unité Scientifique de Nançay of the Observatoire de Paris, associated with the CNRS. The Nançay Observatory acknowledges the financial support of the Région Centre in France. The 22 m Pushchino radio telescope is supported by the Ministry of Science and Education of the Russian Federation (facility registration number 01-10). This work was supported by the Russian Foundation for Basic Research (project

code 09-02-00963-a). The authors are grateful to the staff of the Nançay and Pushchino Radio Astronomy Observatories for their help with the observations and to the anonymous referee for useful comments that helped to improve the paper. This research has made use of the SIMBAD database, operated at CDS, Strasbourg, France

References

Argon, A. L., Reid, M. J., & Menten, K. M. 2000, ApJS, 129, 159
Burdyuzha, V. V. & Varshalovich, D. A. 1973, Soviet Astron., 16, 597
Caswell, J. L., Green, J. A., & Phillips, C. J. 2013, MNRAS, 431, 1180
Colom, P., Lekht, E. E., Pashchenko, M. I., & Rudnitskii, G. M. 2012, Astron. Rep., 56, 731
Fish, V. L., Reid, M. J., Argon, A. L., & Menten, K. M. 2003, ApJ, 596, 328
Forster, J. R. & Caswell, J. L. 1989, A&A, 213, 339
Forster, J. R. & Caswell, J. L. 1999, A&AS, 137, 43
Gardner, F. F., Wilson, T. L., & Thomasson, P. 1975, Astrophys. Lett., 16, 29
Genzel, R. & Downes, D. 1977, A&AS, 30, 145
Goss, W. M. 1968, ApJS, 15, 131
Goss, W. M., Matthews, H. E., & Winnberg, A. 1978, A&A, 65, 307
Goss, W. M. & Shaver, P. A. 1970, Austral. J. Phys. Astrophys. Suppl., 14, 1
Haschick, A. D. & Ho, P. T. P. 1983, ApJ, 267, 638
Immer, K., Reid, M. J., Menten, K. M., Brunthaler, A., & Dame, T. M. 2013, A&A, 553, A117
Jaffe, D. T., Güsten, R., & Downes, D. 1981, ApJ, 250, 621
Kolpak, M. A., Jackson, J. M., Bania, T. M., Clemens, D. P., & Dickey, J. M. 2003, ApJ, 582, 756
Lada, C. J., Blitz, L., Reid, M. J., & Moran, J. M. 1981, ApJ, 243, 769
Lekht, E. E., Pashchenko, M. I., & Rudnitskii, G. M. 2012, Astron. Rep., 56, 45
Lekht, E. E., Slysh, V. I., & Krasnov, V. V. 2007, Astron. Rep., 51, 967
Menten, K. M. 1991, ApJ, 380, L75
Pandian, J. D., Momjian, E., & Goldsmith, P. F. 2008, A&A, 486, 191
Pashchenko, M. I. 1980, Soviet Astron. Lett., 6, 58
Pashchenko, M. I., Rudnitskiĭ, G. M., & Colom, P. 2009, Astron. Rep., 53, 541
Quireza, C., Rood, R. T., Balser, D. S., & Bania, T. M. 2006, ApJS, 165, 338
Robinson, B. J., Goss, W. M., & Manchester, R. N. 1970, Austral. J. Phys., 23, 363
Sato, M., Wu, Y. W., Immer, K., et al. 2014, ApJ, 793, 72
Slysh, V. I., Pashchenko, M. I., Rudnitskiĭ, G. M., Vitrishchak, V. M., & Colom, P. 2010, Astron. Rep., 54, 599
Torrelles, J. M., Patel, N. A., Anglada, G., et al. 2003, ApJ, 598, L115
Zheng, X.-W. 1991, Chin. J. Space Sci., 11, 1

List of Objects

‘W33’ on page 1
‘G12.80−0.20’ on page 1
‘G12.68−0.18’ on page 1
‘G12.80−0.18’ on page 1
‘W33’ on page 1
‘G12.68−0.18’ on page 1
‘G12.80−0.20’ on page 1
‘G12.91−0.28’ on page 1
‘W33B’ on page 5

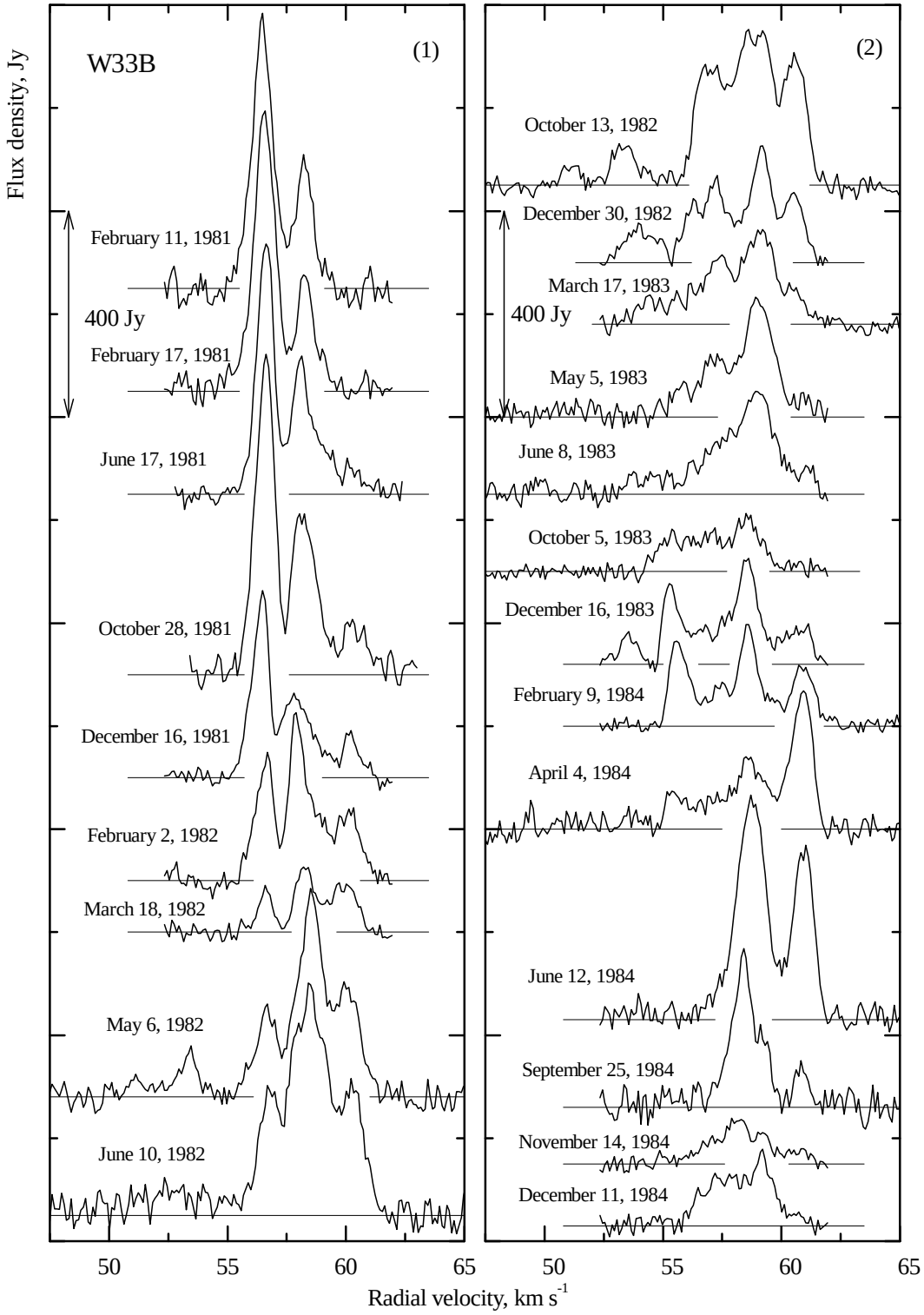

Fig. 7. Spectra of the H_2O maser emission in W33B.

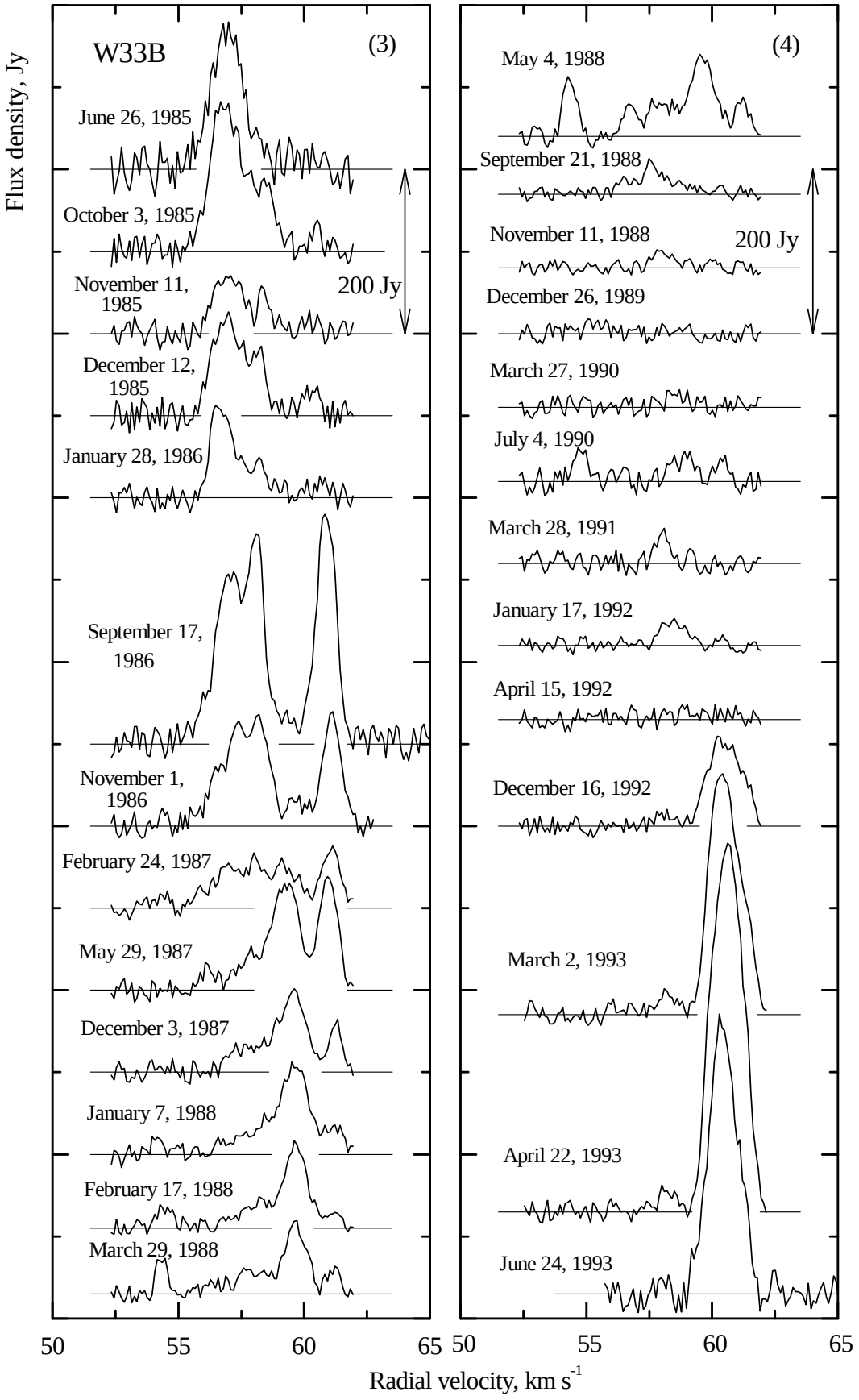

Fig. 7. Continued.

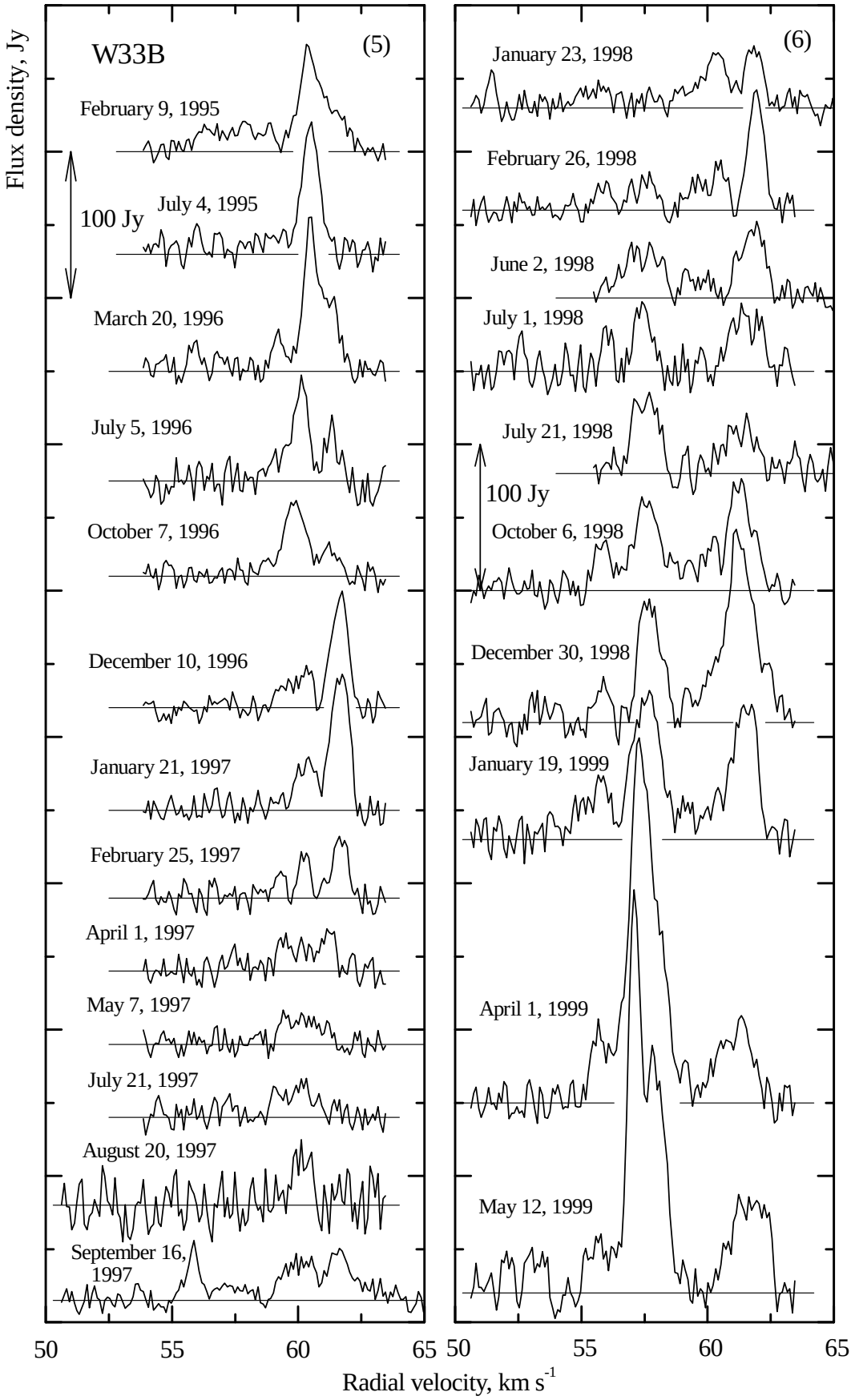

Fig. 7. Continued.

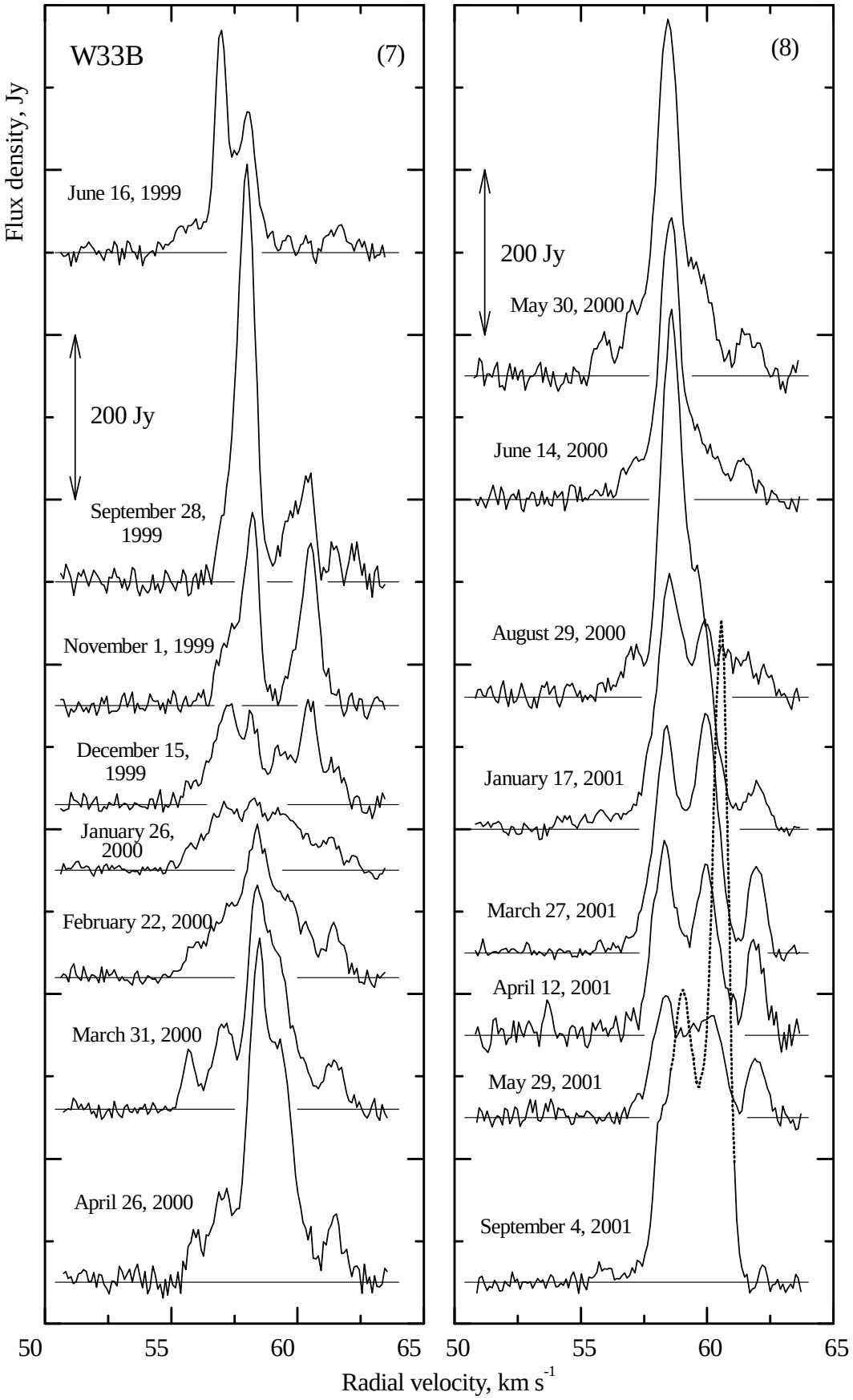

Fig. 7. Continued.

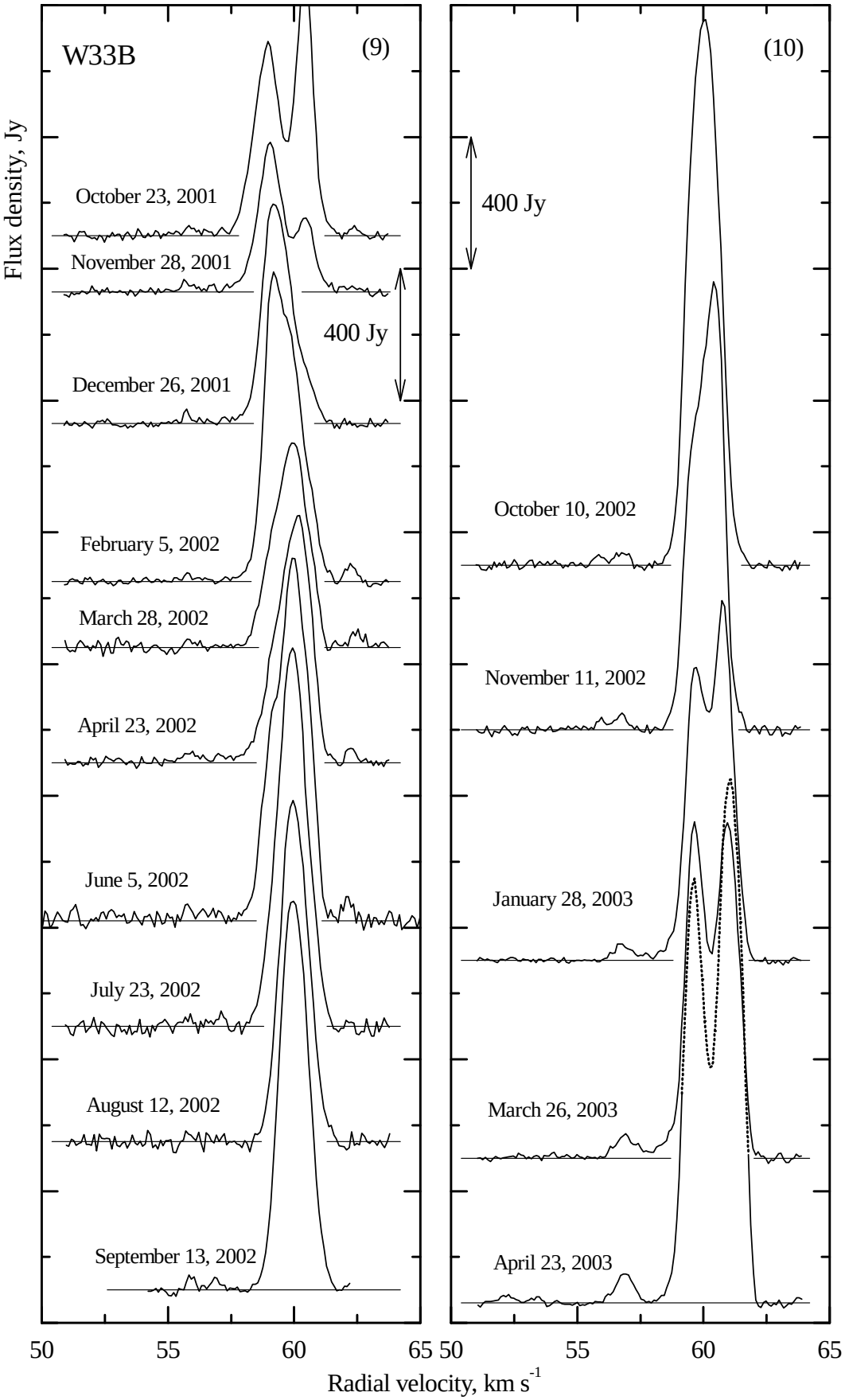

Fig. 7. Continued.

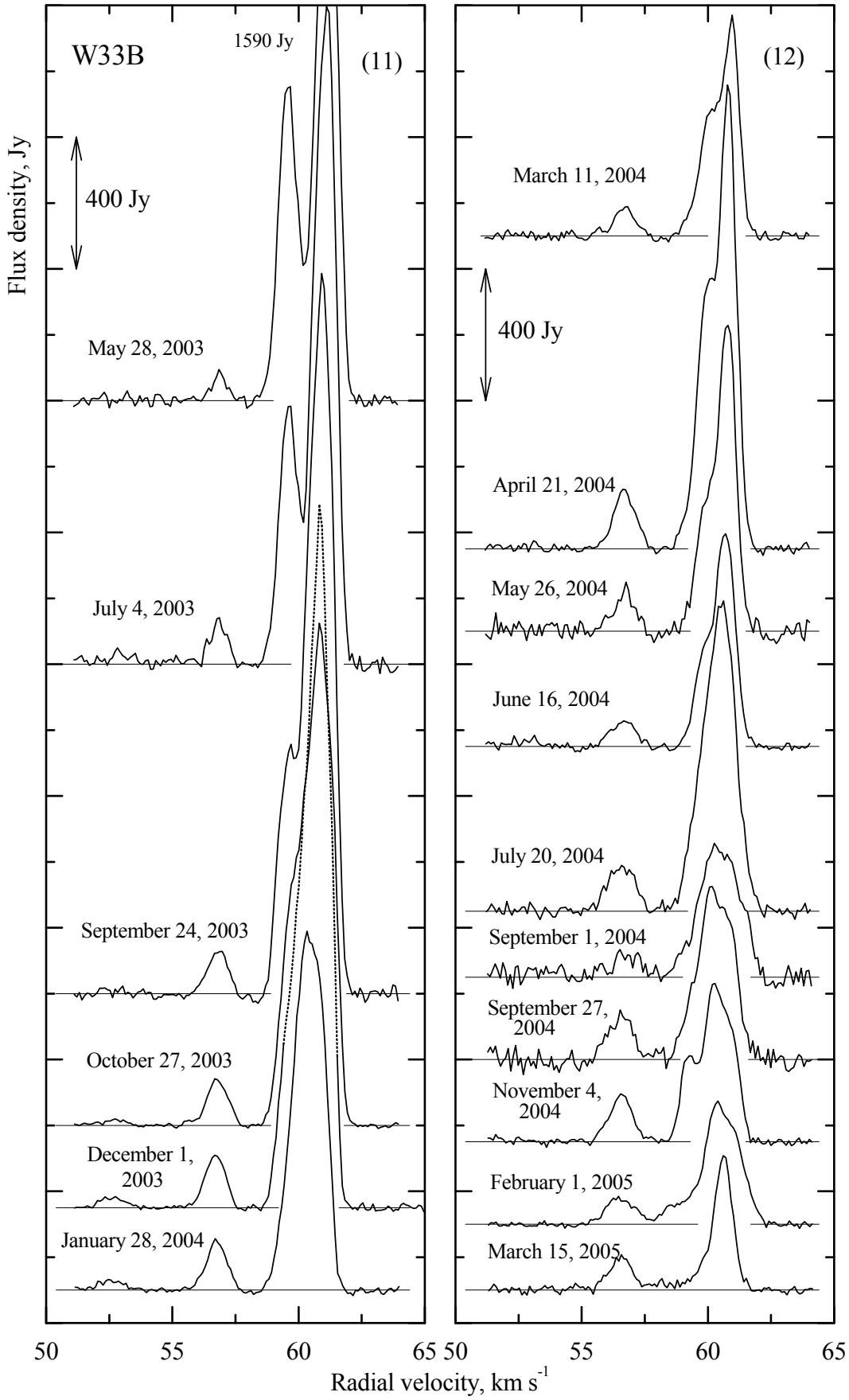

Fig. 7. Continued.

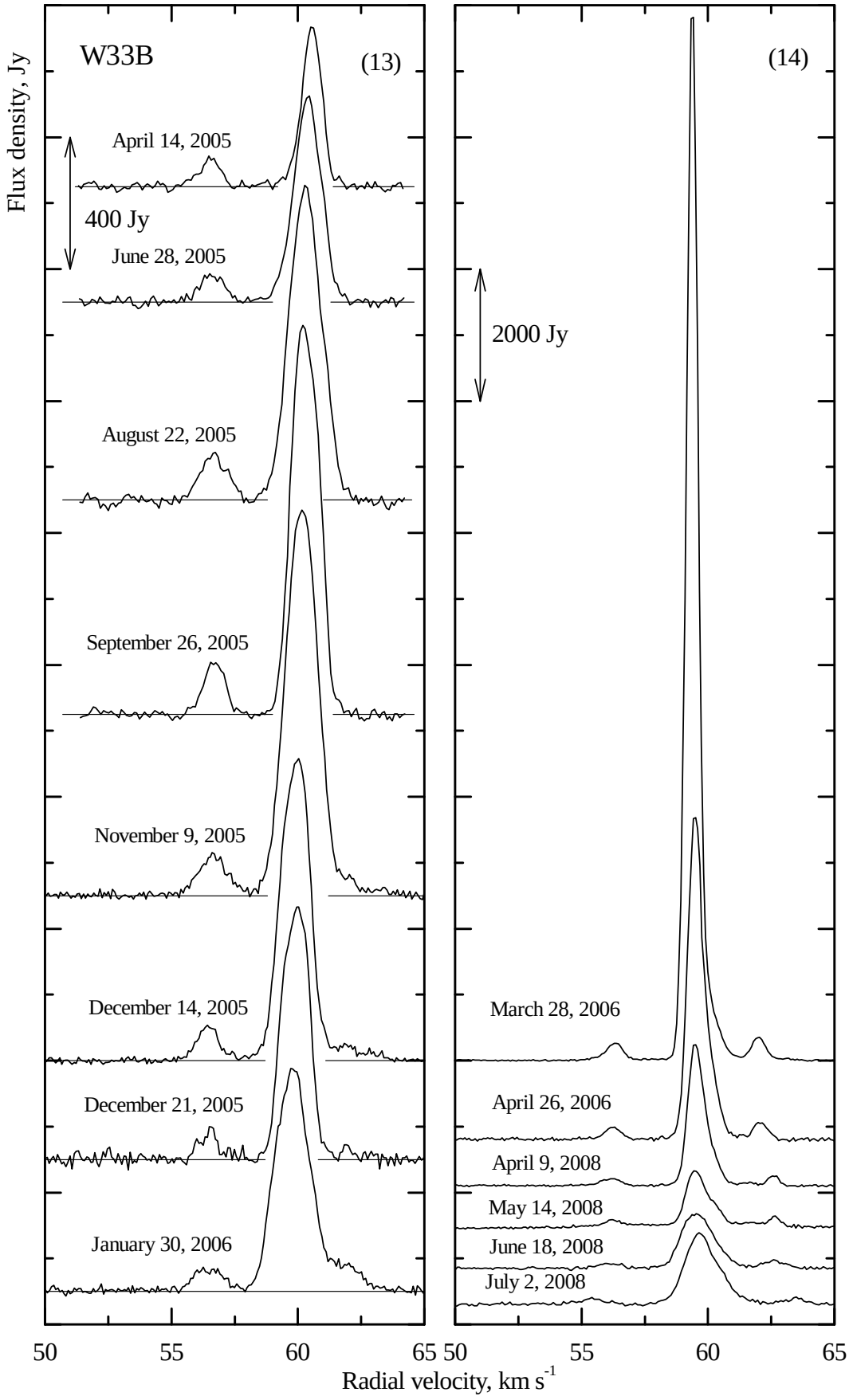

Fig. 7. Continued.

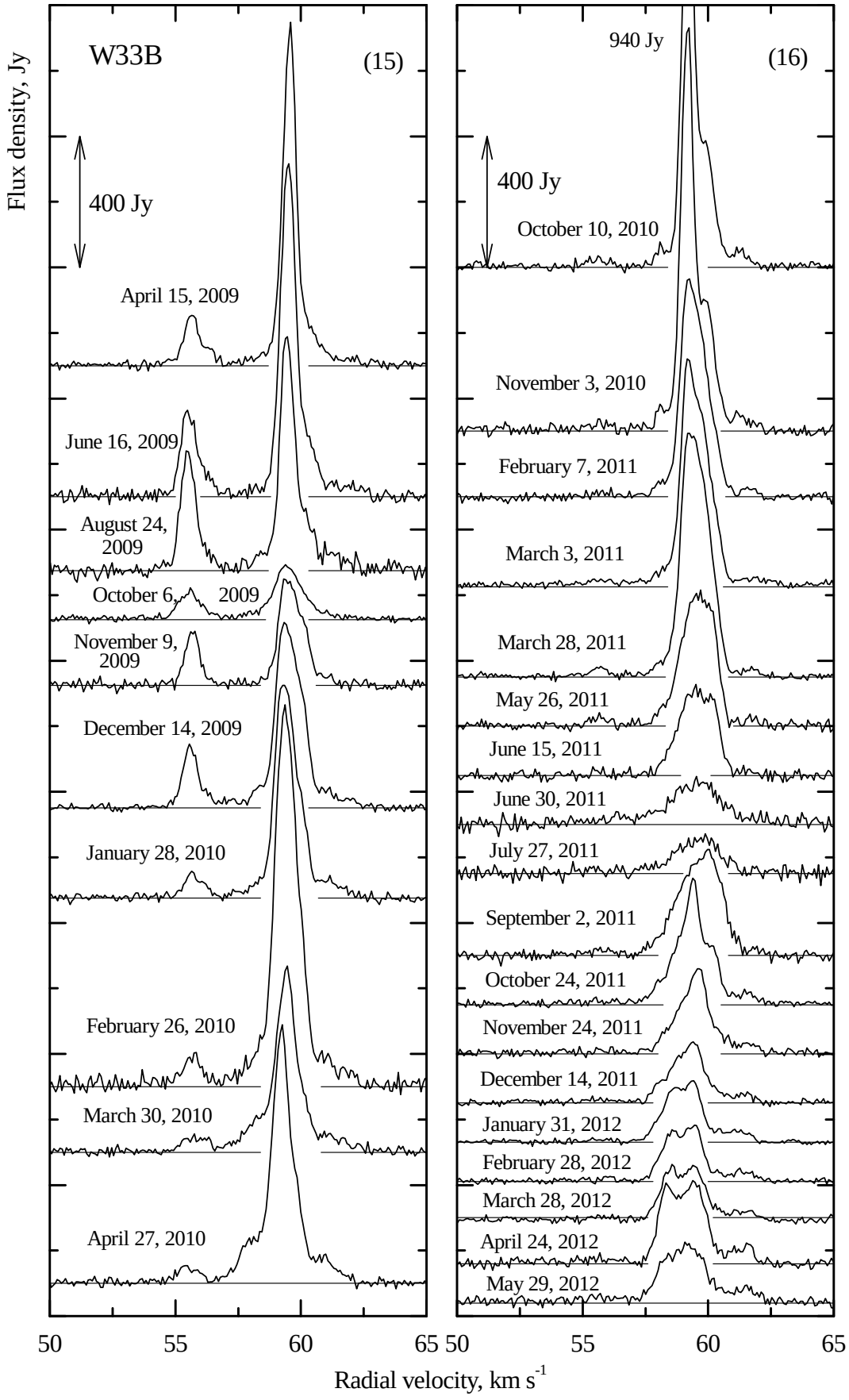

Fig. 7. Continued.

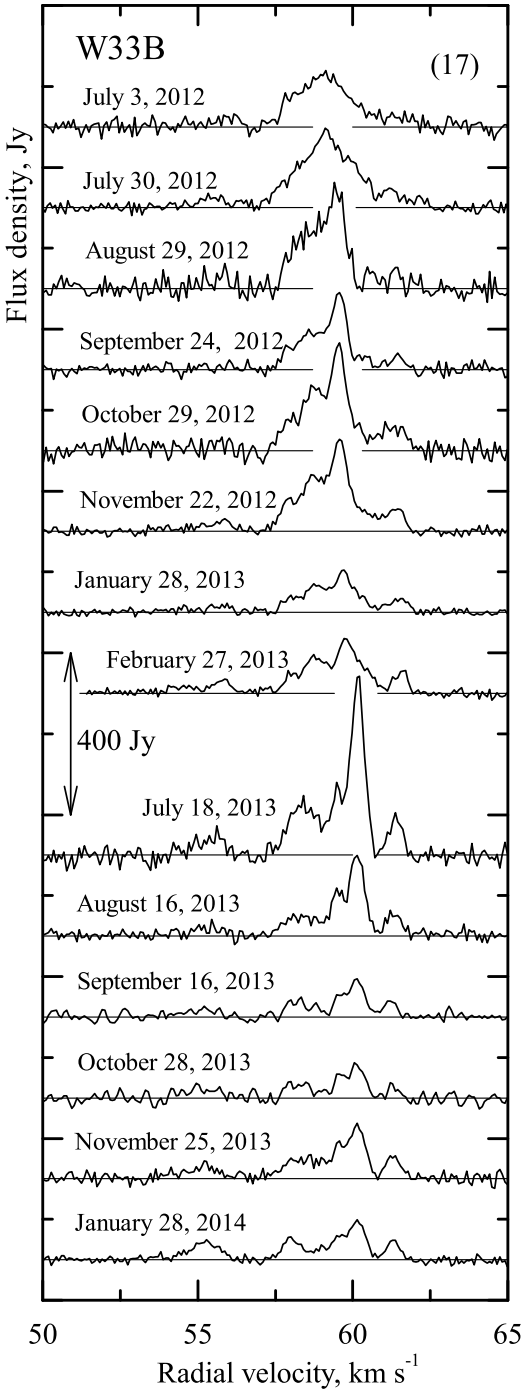

Fig. 7. Continued.